Supporting Information

Advanced Theoretical Design of Light-Driven Molecular Rotary Motors: Enhancing Thermal Helix Inversion and Visible-Light Activation

Weiliang Shi,[a] Jianzheng Ma,[b] Chenwei Jiang,[b] * and Tetsuya Taketsugu[c,d] *

[a] Graduate School of Chemical Sciences and Engineering, Hokkaido University, Sapporo 060-0810, Japan

[b] Ministry of Education Key Laboratory for Nonequilibrium Synthesis and Modulation of Condensed Matter, Shaanxi Province Key Laboratory of Quantum Information and Quantum Optoelectronic Devices, School of Physics, Xi'an Jiaotong University, Xi'an 710049, China

[c] Department of Chemistry, Faculty of Science, Hokkaido University, Sapporo 060-0810, Japan

[d] Institute for Chemical Reaction Design and Discovery (WPI-ICReDD), Hokkaido University, Sapporo 001-0021, Japan

Chenwei Jiang: jiangcw@xjtu.edu.cn,Tetsuya Taketsugu: take@sci.hokudai.ac.jp

Table of contents

1. Key structures along the reaction pathway of molecule 1s

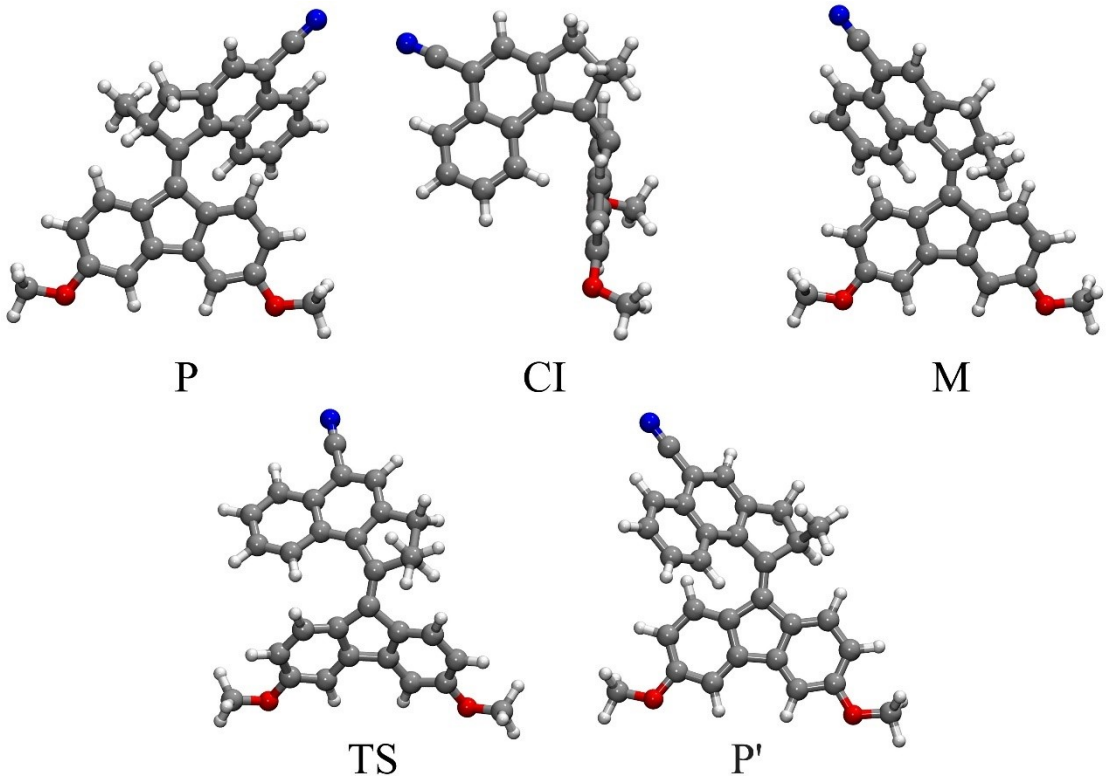

Figure S1. Optimized structures of minima, one conical intersection, and one transition state along the reaction pathway of molecule 1s calculated at the OM2/MRCI level.

Table S1. Geometrical parameters of optimized equilibrium and transition state structures in the ground state for 1s, calculated by the OM2/MRCI method, using the MNDO99 program,[1] and by B3LYP-D3, CAMB3LYP-D3, M06-2X, and ωB97XD methods with 6-31G(d,p) basis sets, using the Gaussian09 program.[2] The bond lengths are given in Å, while bond angles and dihedral angles are given in degrees.

		OM2/MRCI	B3LYP-D3	CAMB3LYP-D3	M06-2X	ωB97XD
P	C1-C2	1.35804	1.36772	1.3547	1.35744	1.35552
	C40-C2-C1	126.9	126.535	126.386	126.096	126.427
	C2-C1-C4	125.904	124.632	124.769	124.59	125.032
	C40-C2-C1-C4	21.785	21.118	20.416	19.829	20.451
	C40-C2-C1-C15	-170.138	-169.548	-170.758	-170.663	-171.08
	C2-C28-C40-C1	-0.527	-1.359	-1.35	-1.507	-1.365
	C2-C1-C15-C17	40.462	40.548	41.468	40.602	42.032
M	C1-C2	1.36331	1.3761	1.36139	1.36391	1.36196
	C40-C2-C1	127.978	127.949	128.215	128.366	128.128
	C2-C1-C4	124.41	124.504	125.061	124.928	125.402
	C40-C2-C1-C4	147.441	145.218	146.286	146.458	145.783
	C40-C2-C1-C15	-25.392	-29.015	-27.457	-26.842	-27.091
	C2-C28-C40-C1	-1.381	-1.183	-1.202	-1.38	-1.275
	C2-C1-C15-C17	-26.879	-27.786	-29.552	-29.826	-30.36
TS	C1-C2	1.36446	1.38357	1.36968	1.37336	1.37064
	C40-C2-C1	120.986	122.114	121.732	121.299	121.68
	C2-C1-C4	117.947	117.969	117.835	117.555	117.85
	C40-C2-C1-C4	-24.731	-24.094	-22.119	-21.646	-22.346
	C40-C2-C1-C15	142.51	139.727	144.791	145.794	144.687
	C2-C28-C40-C1	-9.315	-8.102	-8.168	-8.204	-8.312
	C2-C1-C15-C17	19.901	23.183	22.516	20.848	22.417
P'	C1-C2	1.35804	1.36772	1.3547	1.35744	1.35552
	C40-C2-C1	127.6	128.319	128.66	128.724	128.576
	C2-C1-C4	125.903	124.632	124.769	124.59	125.032
	C40-C2-C1-C4	-156.883	-155.427	-156.12	-156.326	-156.049
	C40-C2-C1-C15	11.203	13.907	12.706	13.182	12.419
	C2-C28-C40-C1	0.526	1.359	1.35	1.507	1.365
	C2-C1-C15-C17	40.461	40.548	41.468	40.602	42.032

Table S2. Geometrical parameters of the CI structure between S_0 and S_1 states for 1s calculated by the OM2/MRCI method. The bond lengths are given in Å, while bond angles and dihedral angles are given in degrees.

CI	C1-C2	1.41331
	C40-C2-C1	96.940
	C2-C1-C4	115.996
	C40-C2-C1-C4	-112.117
	C40-C2-C1-C15	54.979
	C2-C28-C40-C1	-35.041
	C2-C1-C15-C17	19.312

Table S3. Energies of the relevant structures in the ground state for 1s, calculated by the OM2/MRCI method (in eV), and by the B3LYP-D3, CAMB3LYP-D3, M06-2X, and ωB97XD methods with 6-31G(d,p) basis sets (in Hartree). The energies relative to P are also given in parenthesis (in kcal/mol).

	OM2/MRCI	B3LYP-D3	CAMB3LYP-D3	M062X	ωB97XD
P	-5045.166	-1362.32954	-1361.56497	-1361.70764	-1361.82290
M	-5045.081 (2.0)	-1362.32354 (3.8)	-1361.55784 (4.5)	-1361.70076 (4.3)	-1361.81584 (4.4)
TS	-5044.222 (21.8)	-1362.28838 (25.8)	-1361.52354 (26.0)	-1361.66602 (26.1)	-1361.78155 (26.0)

2. Key structures along the reaction pathway of molecule 2s

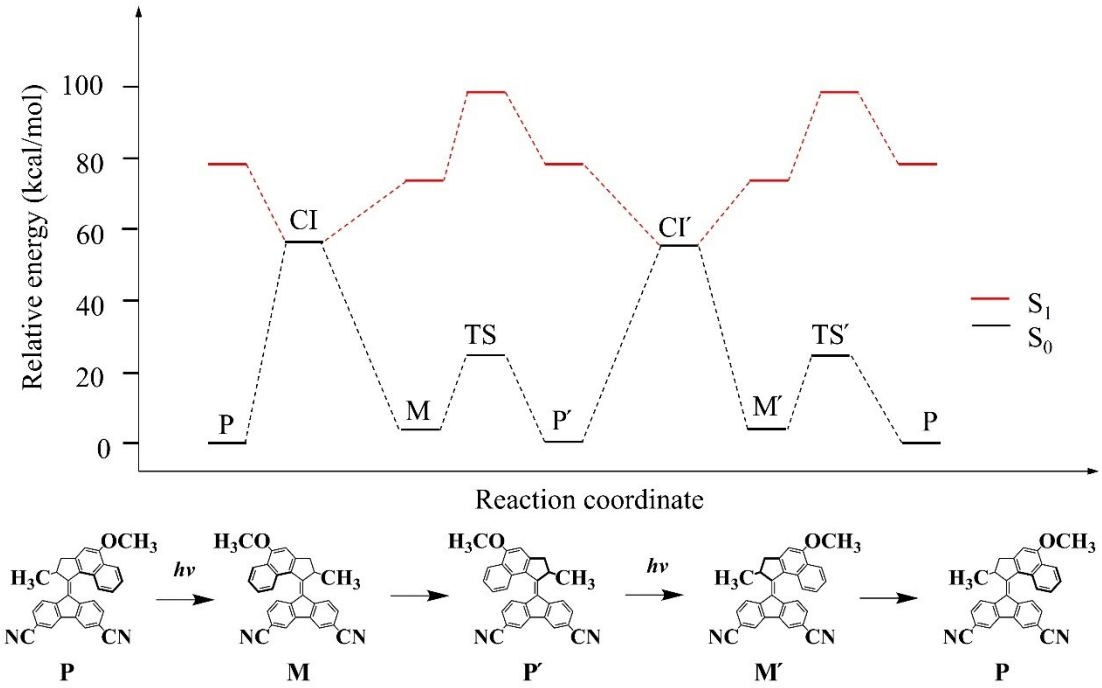

Figure S2. The energy profiles of S_0 and S_1 states of a rotation cycle for the molecule 2s (P → M→ P' → M' → P) at the OM2/MRCI level; CI and TS denote conical intersection and transition state, respectively.

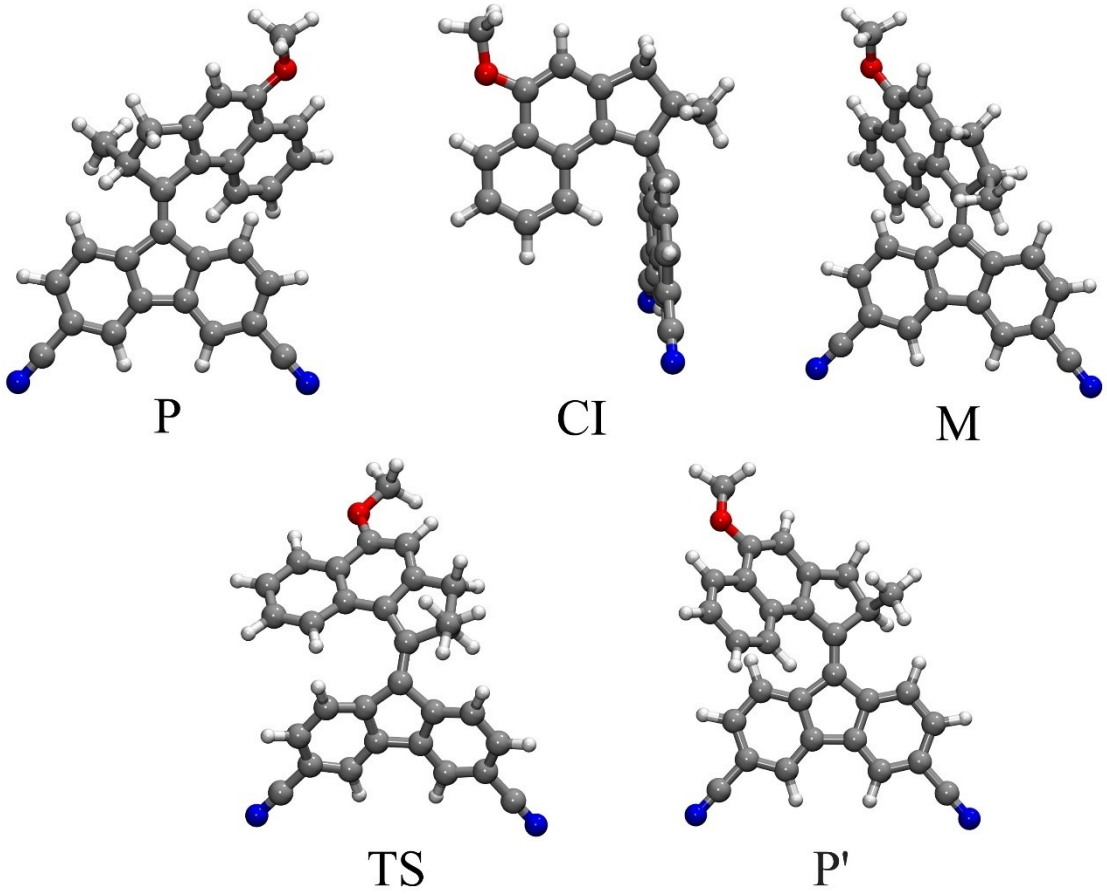

Figure S3. Optimized structures of minima, one conical intersection, and one transition state along the reaction pathway of molecule 2s calculated at the OM2/MRCI level.

Table S4. Geometrical parameters of optimized equilibrium and transition state structures in the ground state for 2s, calculated by the OM2/MRCI method, using the MNDO99 program,[1] and by B3LYP-D3, CAMB3LYP-D3, M06-2X, and ωB97XD methods with 6-31G(d,p) basis sets, using the Gaussian09 program.[2] The bond lengths are given in Å, while bond angles and dihedral angles are given in degrees.

		OM2/MRCI	B3LYP-D3	CAM-B3LYP-D3	M06-2X	ωB97XD
P	C1-C2	1.36244	1.37408	1.36111	1.36373	1.36217
	C40-C2-C1	127.136	126.811	126.682	126.466	126.733
	C2-C1-C4	125.498	124.365	124.468	124.204	124.61
	C40-C2-C1-C4	21.189	21.188	20.288	19.633	20.533
	C40-C2-C1-C15	-169.491	-167.68	-168.969	-169.132	-168.652
	C2-C28-C40-C1	-0.94	-1.486	-1.542	-1.686	-1.297
	C2-C1-C15-C17	39.236	37.796	38.809	37.881	38.548
M	C1-C2	1.367	1.38365	1.3698	1.37196	1.37077
	C40-C2-C1	127.561	127.504	127.705	127.775	127.747
	C2-C1-C4	124.112	123.731	124.076	123.962	124.088
	C40-C2-C1-C4	146.833	144.009	145.301	145.919	145.078
	C40-C2-C1-C15	-26.653	-30.574	-29.107	-28.197	-28.967
	C2-C28-C40-C1	-1.713	-1.343	-1.319	-1.293	-1.425
	C2-C1-C15-C17	-26.159	-25.278	-26.561	-26.616	-26.635
TS	C1-C2	1.37	1.39052	1.37641	1.37956	1.37751
	C40-C2-C1	121.347	121.658	121.385	121.007	121.391
	C2-C1-C4	117.714	117.878	117.644	117.349	117.701
	C40-C2-C1-C4	-25.973	-25.947	-24.752	-23.953	-25.633
	C40-C2-C1-C15	140.72	139.347	142.667	143.871	141.809
	C2-C28-C40-C1	-9.361	-9.179	-9.323	-9.34	-9.508
	C2-C1-C15-C17	19.445	21.305	20.293	19.016	19.298
P'	C1-C2	1.36243	1.37408	1.36112	1.36373	1.36217
	C40-C2-C1	127.214	127.734	128.023	128.027	127.944
	C2-C1-C4	125.499	124.365	124.468	124.204	124.61
	C40-C2-C1-C4	-156.435	-155.071	-155.798	-156.111	-156.18
	C40-C2-C1-C15	12.872	16.061	14.945	15.125	14.636
	C2-C28-C40-C1	0.949	1.486	1.543	1.687	1.297
	C2-C1-C15-C17	39.256	37.796	38.809	37.88	38.547

Table S5. Geometrical parameters of the CI structure between S_0 and S_1 states for 2s calculated by the OM2/MRCI method. The bond lengths are given in Å, while bond angles and dihedral angles are given in degrees.

CI	C1-C2	1.41136
	C40-C2-C1	116.416
	C2-C1-C4	118.624
	C40-C2-C1-C4	-115.421
	C40-C2-C1-C15	61.837
	C2-C28-C40-C1	-25.085
	C2-C1-C15-C17	3.152

Table S6. Energies of the relevant structures in the ground state for 2s, calculated by the OM2/MRCI method (in eV), and by the B3LYP-D3, CAMB3LYP-D3, M06-2X, and ωB97XD methods with 6-31G(d,p) basis sets (in Hartree). The energies relative to P are also given in parenthesis (in kcal/mol).

	OM2/MRCI	B3LYP-D3	CAMB3LYP-D3	M062X	ωB97XD
P	-4882.130	-1340.04773	-1339.28776	-1339.44615	-1339.54261
M	-4882.057 (1.7)	-1340.04351 (2.7)	-1339.28239 (3.4)	-1339.44095 (3.3)	-1339.53729 (3.3)
TS	-4881.165 (22.3)	-1340.00606 (26.2)	-1339.24581 (26.3)	-1339.40409 (26.4)	-1339.50077 (26.3)

3. Key structures along the reaction pathway of molecule 6s

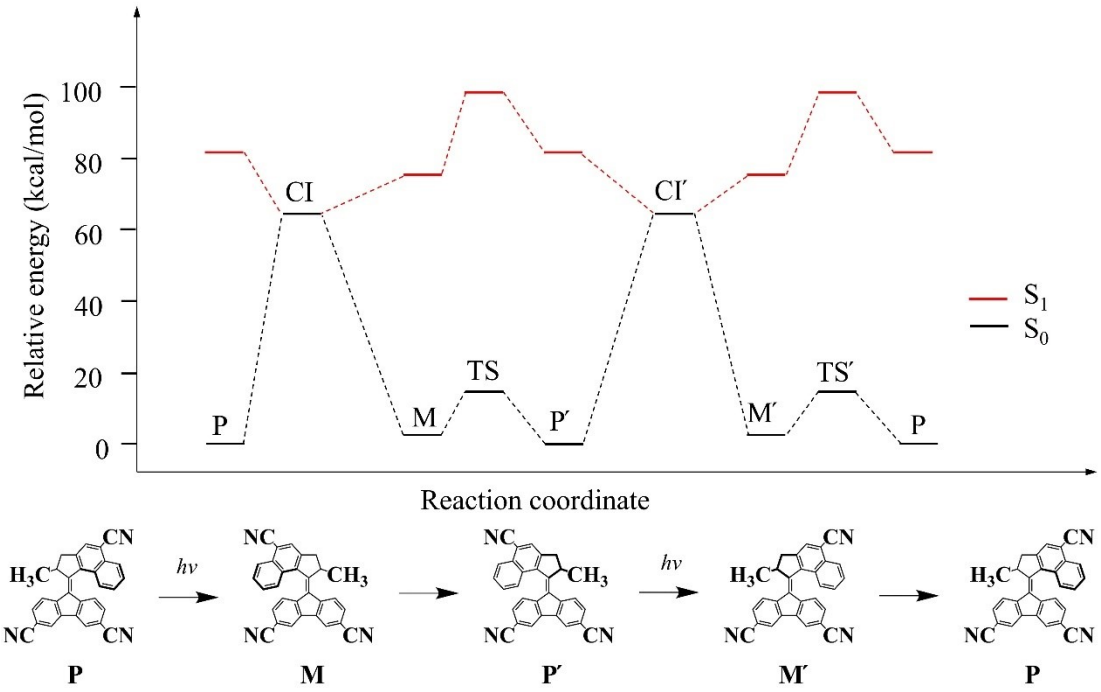

Figure S4. The energy profiles of S_0 and S_1 states of a rotation cycle for the molecule 6s (P → M→ P' → M' → P) at the OM2/MRCI level; CI and TS denote conical intersection and transition state, respectively.

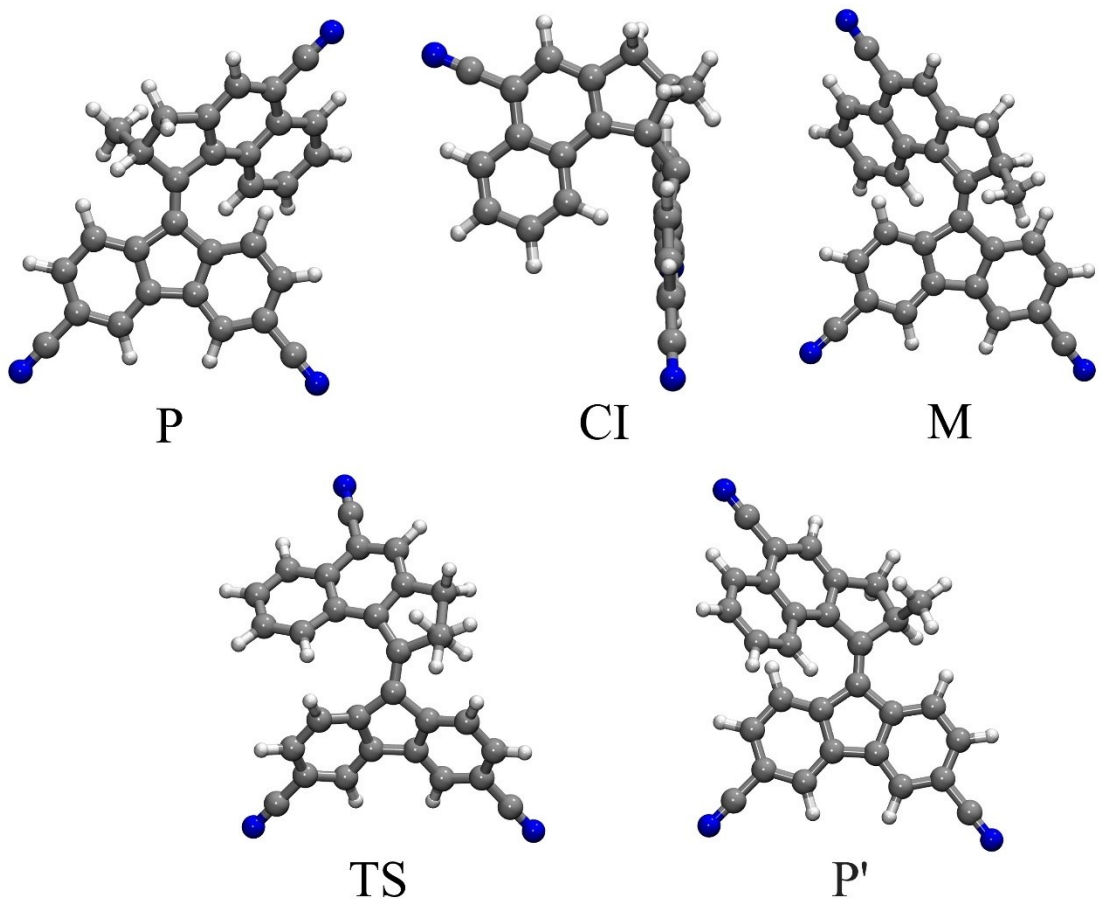

Figure S5. Optimized structures of minima, one conical intersection, and one transition state along the reaction pathway of molecule 6s calculated at the OM2/MRCI level.

Table S7. Geometrical parameters of optimized equilibrium and transition state structures in the ground state for 6s, calculated by the OM2/MRCI method, using the MNDO99 program,[1] and by B3LYP-D3, CAMB3LYP-D3, M06-2X, and ωB97XD methods with 6-31G(d,p) basis sets, using the Gaussian09 program.[2] The bond lengths are given in Å, while bond angles and dihedral angles are given in degrees.

		OM2/MRCI	B3LYP-D3	CAM-B3LYP-D3	M06-2X	WB97XD
P	C1-C2	1.35898	1.36989	1.35707	1.35968	1.35804
	C40-C2-C1	126.835	126.579	126.42	126.241	126.426
	C2-C1-C4	125.955	124.703	124.834	124.667	124.999
	C40-C2-C1-C4	21.6	21.599	20.799	20.296	20.941
	C40-C2-C1-C15	-169.998	-168.293	-169.6	-169.462	-169.603
	C2-C28-C40-C1	-0.882	-1.347	-1.405	-1.44	-1.294
	C2-C1-C15-C17	40.284	39.438	40.506	39.352	40.588
M	C1-C2	1.36383	1.3787	1.36441	1.36678	1.36501
	C40-C2-C1	127.85	127.689	127.928	128.025	127.857
	C2-C1-C4	124.585	124.304	124.786	124.65	125.075
	C40-C2-C1-C4	146.698	144.398	145.497	146.125	144.741
	C40-C2-C1-C15	-26.35	-29.937	-28.508	-27.649	-28.44
	C2-C28-C40-C1	-1.707	-1.211	-1.24	-1.191	-1.479
	C2-C1-C15-C17	-26.792	-26.783	-28.357	-28.262	-29.206
TS	C1-C2	1.36663	1.38642	1.37254	1.37609	1.37341
	C40-C2-C1	121.58	121.673	121.396	120.999	121.469
	C2-C1-C4	118.444	118.203	117.954	117.69	118.095
	C40-C2-C1-C4	-24.553	-25.939	-24.65	-24.364	-26.086
	C40-C2-C1-C15	140.401	138.229	141.927	142.268	139.706
	C2-C28-C40-C1	-8.77	-8.808	-8.871	-8.964	-9.125
	C2-C1-C15-C17	21.484	22.235	21.217	19.69	20.136
P'	C1-C2	1.35898	1.36989	1.36989	1.35968	1.35804
	C40-C2-C1	127.541	128.028	128.028	128.329	128.304
	C2-C1-C4	125.958	124.703	124.703	124.667	124.998
	C40-C2-C1-C4	-156.177	-154.997	-154.997	-156.057	-155.769
	C40-C2-C1-C15	12.228	15.112	15.112	14.186	13.688
	C2-C28-C40-C1	0.879	1.347	1.347	1.44	1.294
	C2-C1-C15-C17	40.287	39.438	39.438	39.353	40.588

Table S8. Geometrical parameters of the CI structure between S_0 and S_1 states for 6s, calculated by the OM2/MRCI method. The bond lengths are given in Å, while bond angles and dihedral angles are given in degrees.

CI	C1-C2	1.41232
	C40-C2-C1	103.484
	C2-C1-C4	116.705
	C40-C2-C1-C4	-114.918
	C40-C2-C1-C15	55.426
	C2-C28-C40-C1	-32.841
	C2-C1-C15-C17	12.953

Table S9. Energies of the relevant structures in the ground state for 6s, calculated by the OM2/MRCI method (in eV), and by the B3LYP-D3, CAMB3LYP-D3, M06-2X, and ωB97XD methods with 6-31G(d,p) basis sets (in Hartree). The energies relative to P are also given in parenthesis (in kcal/mol).

	OM2/MRCI	B3LYP-D3	CAMB3LYP-D3	M062X	ωB97XD
P	-4718.473	-1317.75644	-1317.00065	-1317.17537	-1317.25304
M	-4718.389 (1.9)	-1317.75117 (3.3)	-1316.99421 (4.0)	-1317.16911 (3.9)	-1317.24659 (4.0)
TS	-4717.522 (21.9)	-1317.71460 (26.3)	-1316.95834 (26.5)	-1317.13286 (26.7)	-1317.21080 (26.5)

4. Key structures along the reaction pathway of molecule Xs

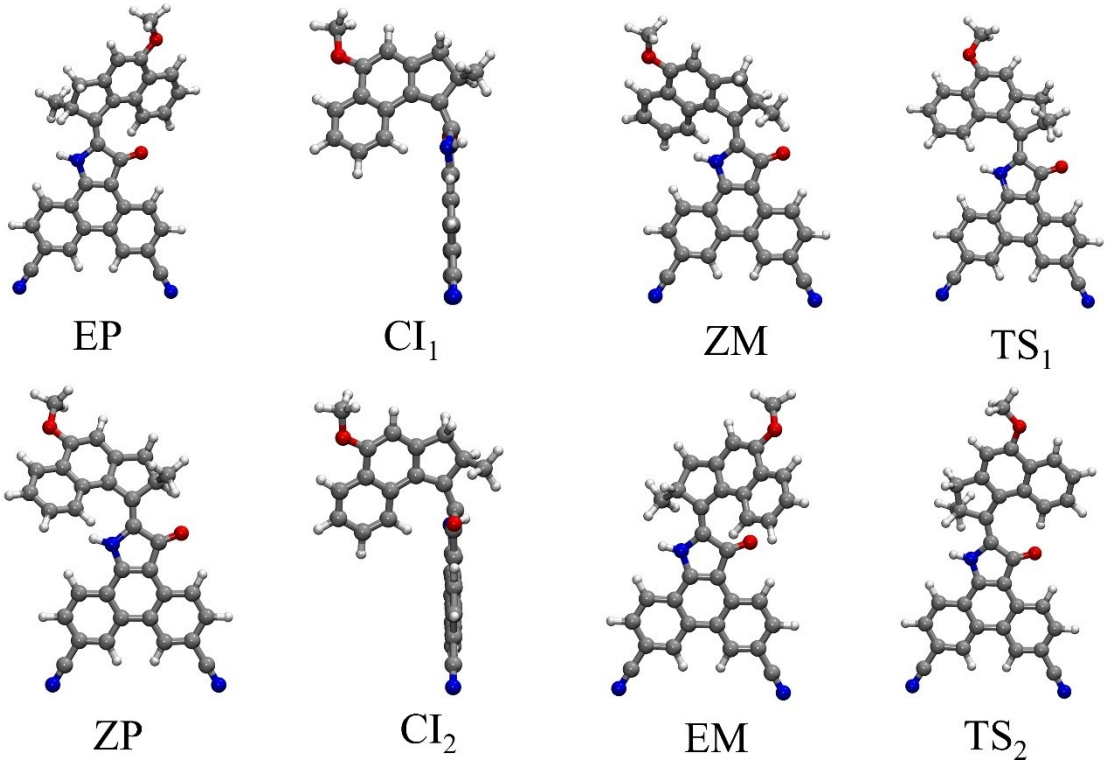

Figure S6. Optimized structures of minima, conical intersections, and transition states along the reaction pathway of molecule Xs calculated at the OM2/MRCI level.

Table S10. Geometrical parameters of optimized equilibrium and transition state structures in the ground state for Xs, calculated by the OM2/MRCI method, using the MNDO99 program,[1] and by B3LYP-D3, CAMB3LYP-D3, M06-2X, and ωB97XD methods with 6-31G(d,p) basis sets, using the Gaussian09 program.[2] The bond lengths are given in Å, while bond angles and dihedral angles are given in degrees.

		OM2/MRCI	B3LYP-D3	CAM-B3LYP-D3	M06-2X	WB97XD
EP	C1-C2	1.36942	1.36419	1.35219	1.35451	1.3543
	C40-C2-C1	121.753	122.046	122.228	122.385	121.928
	C2-C1-C4	129.564	130.965	131.198	130.97	131.214
	C40-C2-C1-C4	10.601	10.096	9.477	8.684	9.52
	C40-C2-C1-C15	-177.726	-176.97	-177.985	-179.27	-178.09
	C2-C28-C40-C1	4.06	5.214	5.091	5.511	5.218
	C2-C1-C15-C17	30.966	30.427	31.366	31.89	32.103
ZM	C1-C2	1.36982	1.36793	1.35618	1.35758	1.35802
	C40-C2-C1	123.841	126.638	127.098	123.916	123.588
	C2-C1-C4	125.563	130.516	130.624	125.645	126.056
	C40-C2-C1-C4	163.12	162.916	163.705	160.136	160.544
	C40-C2-C1-C15	-5.823	-7.113	-6.271	-9.365	-9.637
	C2-C28-C40-C1	-1.487	-0.683	-0.67	-1.135	-1.457
	C2-C1-C15-C17	-30.039	-13.217	-13.117	-29.498	-28.605
TS1	C1-C2	1.37169	1.37165	1.36005	1.3624	1.36188
	C40-C2-C1	129.854	128.315	128.556	128.58	128.137
	C2-C1-C4	134.649	135.526	135.399	135.434	135.358
	C40-C2-C1-C4	-179.489	-177.662	-178.657	-179.469	-177.655
	C40-C2-C1-C15	-5.088	-4.575	-3.711	-2.785	-4.958
	C2-C28-C40-C1	-2.398	-3.361	-3.566	-3.971	-3.793
	C2-C1-C15-C17	17.746	12.818	13.355	12.946	14.367
ZP	C1-C2	1.36593	1.36178	1.35035	1.35287	1.35223
	C40-C2-C1	126.864	126.493	126.903	127.077	126.389
	C2-C1-C4	128.289	129.523	129.547	129.44	129.162
	C40-C2-C1-C4	-170.801	-168.852	-169.122	-169.133	-169.63
	C40-C2-C1-C15	-4.392	1.501	1.182	0.826	-0.04
	C2-C28-C40-C1	0.09	-1.672	-1.634	-2.086	-1.752
	C2-C1-C15-C17	33.045	27.369	27.583	27.084	28.015
EM	C1-C2	1.37008	1.36667	1.35423	1.35638	1.35703
	C40-C2-C1	124.427	124.101	124.568	124.636	124.16
	C2-C1-C4	125.925	127.795	127.852	127.672	127.634
	C40-C2-C1-C4	-15.286	-15.552	-14.147	-14.313	-15.487
	C40-C2-C1-C15	171.35	170.469	172.936	172.656	170.871
	C2-C28-C40-C1	-3.854	-4.841	-4.687	-4.786	-4.726
	C2-C1-C15-C17	-30.243	-30.551	-33.004	-33.14	-31.639

TS2	C1-C2	1.38233	1.3852	1.37165	1.37442	1.37376
	C40-C2-C1	118.168	117.287	117.477	117.364	117.307
	C2-C1-C4	136.885	138.813	139.096	139.301	138.927
	C40-C2-C1-C4	-5.25	-8.432	-8.136	-7.905	-8.523
	C40-C2-C1-C15	171.155	170.772	171.432	172.254	170.103
	C2-C28-C40-C1	-2.147	-1.858	-2.007	-1.917	-2.227
	C2-C1-C15-C17	13.135	7.982	7.181	7.099	8.624

Table S11. Geometrical parameters of the CI_1 and CI_2 structures between S_0 and S_1 states for Xs, calculated by the OM2/MRCI method. The bond lengths are given in Å, while bond angles and dihedral angles are given in degrees.

		OM2/MRCI
CI_1	C1-C2	1.40915
	C40-C2-C1	124.397
	C2-C1-C4	130.702
	C40-C2-C1-C4	-118.012
	C40-C2-C1-C15	74.254
	C2-C28-C40-C1	21.238
	C2-C1-C15-C17	-8.935
CI_2	C1-C2	1.40818
	C40-C2-C1	125.556
	C2-C1-C4	130.535
	C40-C2-C1-C4	118.805
	C40-C2-C1-C15	-76.244
	C2-C28-C40-C1	-20.878
	C2-C1-C15-C17	12.413

Table S12. Energies of the relevant structures in the ground state for Xs, calculated by the OM2/MRCI method (in eV), and by the B3LYP-D3, CAMB3LYP-D3, M06-2X, and ωB97XD methods with 6-31G(d,p) basis sets (in Hartree). The energies relative to EP are also given in parenthesis (in kcal/mol).

	OM2/MRCI	B3LYP-D3	CAMB3LYP-D3	M062X	ωB97XD
EP	-5823.673	-1584.97270	-1584.09429	-1584.26499	-1584.37052
ZM	-5823.81815 (-3.4)	-1584.97501 (-1.5)	-1584.10671 (-7.8)	-1584.27422 (-5.8)	-1584.38103 (-6.6)
TS1	-5823.645 (0.7)	-1584.96585 (4.3)	-1584.09820 (-2.5)	-1584.26679 (-1.1)	-1584.37327 (-1.7)
ZP	-5823.935 (-6.0)	-1584.98174 (-5.7)	-1584.11394 (-12.3)	-1584.28305 (-11.3)	-1584.38954 (-11.9)
EM	-5823.588 (2.0)	-1584.96833 (2.7)	-1584.10007 (-3.6)	-1584.26987 (-3.1)	-1584.37562 (-3.2)
TS2	-5823.499 (4.0)	-1584.95836 (9.0)	-1584.08996 (2.7)	-1584.25845 (4.1)	-1584.36531 (3.3)

5. Excitation energies of the S_1 state in the gas phase and in a solution of dichloromethane solvent

Table S13. The absorption wavelengths (in nm) and excitation energies (in eV) for the S_1 state of the molecules 1s-P, 2s-P, 6s-P, Xs-EP, and Xs-ZP, calculated by TDDFT and TDDFT(DCM) with PBE0-D3/6-31G(d,p). TDDFT(DCM) refers to the values calculated using the Polarizable Continuum Model (PCM) to include the effects of the dichloromethane (DCM) solvent. The experimental data for 1s-P, 2s-P, and 6s-P measured in DCM solvents[3] are also presented. When comparing the calculated values with experimental data, they generally align well. Specifically, for 2s-P, the results incorporating solvent effects show a particularly close match with experimental values.

	TDDFT	TDDFT(DCM)	Exp.
1s-P	445.28/2.78	463.46/2.68	422/2.94
2s-P	422.21/2.94	447.24/2.77	453/2.74
6s-P	425.22/2.92	443.54/2.79	421/2.95
Xs-EP	482.98/2.57	499.28/2.48	
Xs-ZP	465.76/2.66	487.28/2.54	

6. Excitation energies and oscillator strengths of the higher electronic states

Table S14. Excitation energies (in eV) and oscillator strengths of the electronic states, ranging from S_1 to S_6, for 1s-P, 2s-P, 6s-P, Xs-ZP, and Xs-EP, using the PBE0-D3/6-31G(d,p) level of theory. Based on the oscillator strengths obtained, the primary excited state for is identified as S_1.

	1s-P	2s-P	6s-P	Xs-EP	Xs-ZP
S_1	2.78/0.4930	2.94/0.6858	2.92/0.6656	2.57/0.3928	2.66/0.4190
S_2	2.99/0.0553	3.39/0.0002	3.11/0.0005	2.90/0.2101	3.07/0.1746
S_3	3.55/0.1094	3.76/0.0258	3.46/0.0213	3.15/0.1635	3.17/0.0410
S_4	3.78/0.0453	3.84/0.0149	3.88/0.0298	3.39/0.0286	3.44/0.0109
S_5	3.90/0.0505	4.04/0.0006	3.99/0.0292	3.57/0.1123	3.52/0.0897
S_6	4.02/0.0026	4.15/0.0292	4.04/0.0185	3.74/0.0261	3.78/0.0284

7. UV-vis spectra calculated at the OM2/MRCI level

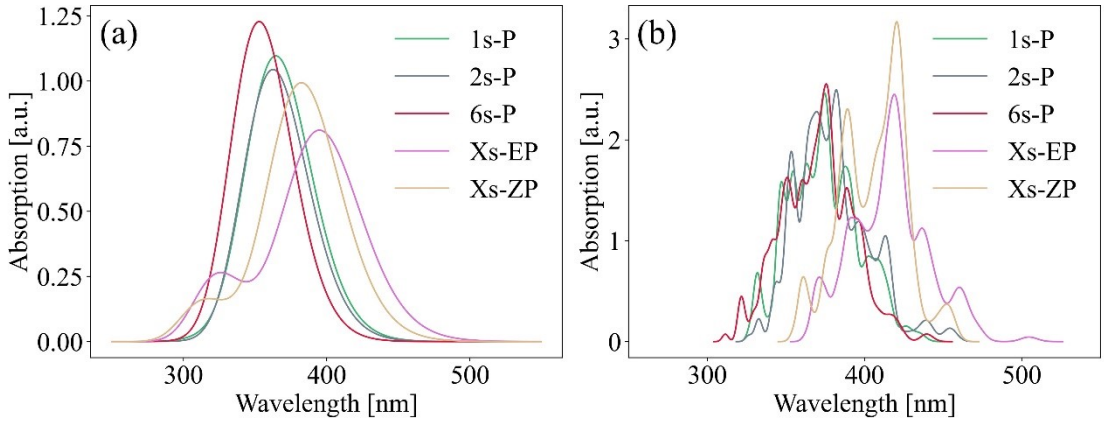

Figure S7. The UV-vis spectra calculated for 1s, 2s, 6s, and Xs at the OM2/MRCI level: (a) generated from the absorption at the equilibrium structure; (b) generated from 200 geometries around equilibrium structures from Wigner sampling. The $S_0 \rightarrow S_1$ excitation energy has been broadened to a full width at half maximum (FWHM) of 0.05 eV using the Newton-X 2.6 program[4].

Figure S7 shows the UV-vis spectra calculated for 1s, 2s, 6s, and Xs at the OM2/MRCI level: (a) generated from the absorption at the equilibrium structure; (b) generated from 200 geometries around equilibrium structures from Wigner sampling. By comparing panels (a) and (b), one can observe the extent to which the absorption spectra are influenced by molecules whose structures are distributed near the equilibrium structure via Wigner sampling. Although multiple peaks appear for each molecule, the peaks showing the maximum absorption intensity do not deviate significantly from the equilibrium structure.

8. Analyses of typical trajectories for 1s, 2s, 6s, and Xs

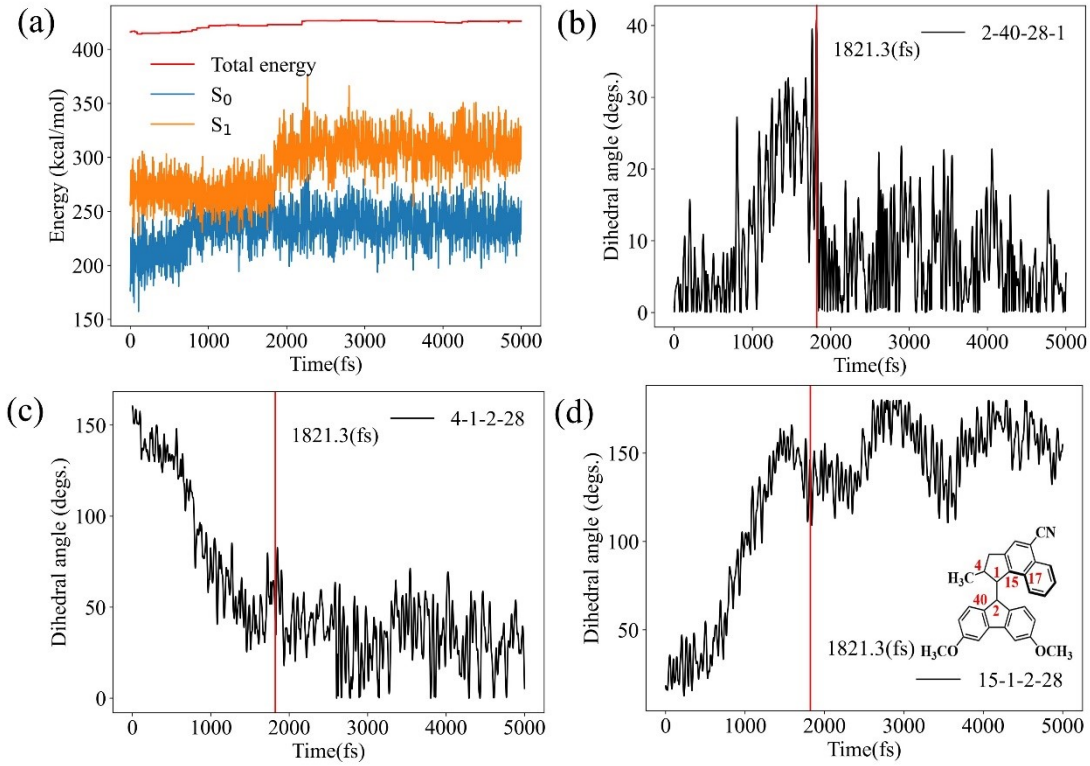

Figure S8. (a) Variation of S_0 and S_1 energies and (b-d) variations of the dihedral angles $\theta_{2\text{-}40\text{-}28\text{-}1}$, $\theta_{4\text{-}1\text{-}2\text{-}28}$, and $\theta_{15\text{-}1\text{-}2\text{-}28}$, along a typical trajectory for 1s. In (a), the total energy is displayed in red. Surface hopping from S_1 to S_0 occurs at 1821.3 fs.

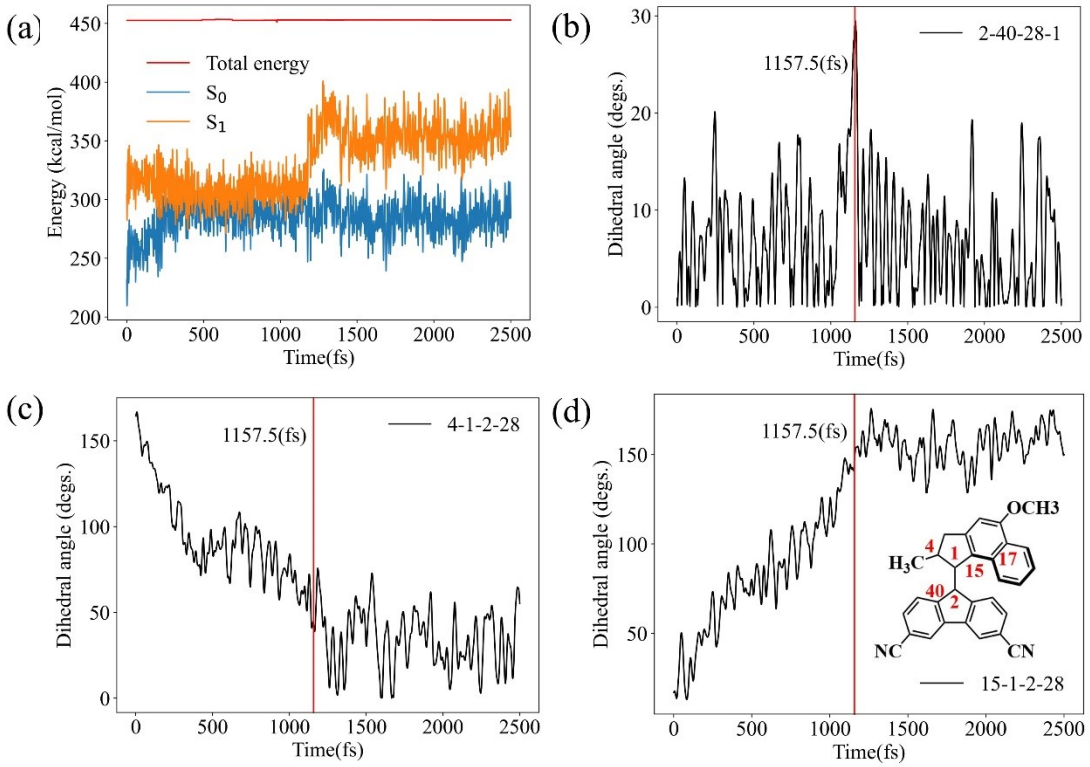

Figure S9. (a) Variation of S_0 and S_1 energies and (b-d) variations of the dihedral angles $\theta_{2\text{-}40\text{-}28\text{-}1}$,

$\theta_{4\text{-}1\text{-}2\text{-}28}$, and $\theta_{15\text{-}1\text{-}2\text{-}28}$, along a typical trajectory for 2s. In (a), the total energy is displayed in red. Surface hopping from S_1 to S_0 occurs at 2949.1 fs.

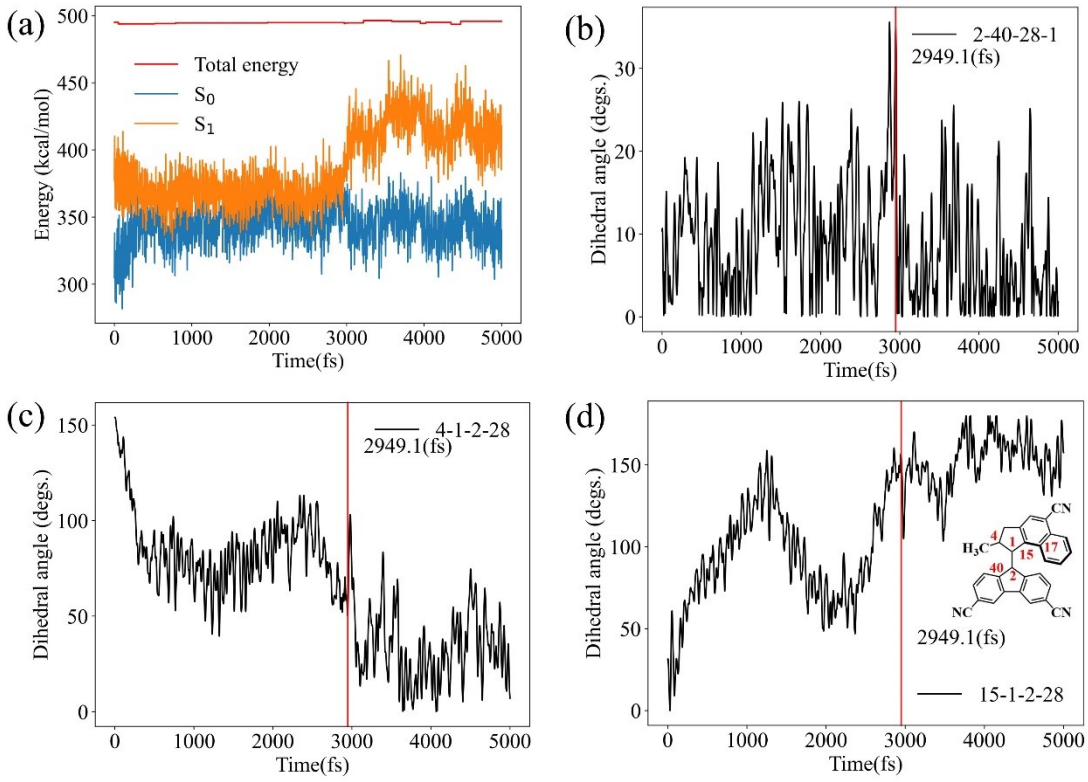

Figure S10. (a) Variation of S_0 and S_1 energies and (b-d) variations of the dihedral angles $\theta_{2\text{-}40\text{-}28\text{-}1}$, $\theta_{4\text{-}1\text{-}2\text{-}28}$, and $\theta_{15\text{-}1\text{-}2\text{-}28}$, along a typical trajectory for 6s. In (a), the total energy is displayed in red. Surface hopping from S_1 to S_0 occurs at 1157.5 fs.

To deepen our understanding of the photoisomerization process in 1s, 2s, and 6s, we have detailed the behavior of crucial angles, specifically, $\theta_{2\text{-}40\text{-}28\text{-}1}$, $\theta_{4\text{-}1\text{-}2\text{-}28}$, and $\theta_{15\text{-}1\text{-}2\text{-}28}$, across characteristic trajectories. These figures reveal the dihedral angles $\theta_{4\text{-}1\text{-}2\text{-}28}$ evolving from initial setups to the conical intersection points at 1821.3, 1157.5 and 2949.1 fs, respectively, before hopping to the S_0 state. Throughout this decay, the dihedral angle $\theta_{4\text{-}1\text{-}2\text{-}28}$ shows a decrease marked by minor fluctuations, in contrast to the dihedral angle $\theta_{15\text{-}1\text{-}2\text{-}28}$, which exhibits a steady increase. Approaching the conical intersection, the angle $\theta_{2\text{-}40\text{-}28\text{-}1}$ shifts abruptly, showing dynamic shifts akin to precessional motion. After internal conversion to the S_0 state, there's a sequential decrease in $\theta_{4\text{-}1\text{-}2\text{-}28}$ and increase in $\theta_{15\text{-}1\text{-}2\text{-}28}$, leading both angles to settle into slight oscillations within the M region - signaling the end of the photoisomerization journey.

In molecular dynamics (MD) simulations, we use the velocity-Verlet algorithm, which largely preserves total energy if appropriate time steps are utilized. However, when performing TSH calculations for excited states based on multi-configurational and multi-reference wavefunctions, structural changes during MD calculations can cause the orbitals within the active

space to swap with outer orbitals, or states included in the state averaging to swap with external states, which can potentially disrupt the conservation of total energy. In this study, using the OM2/MRCI method, we observe cases where energy conservation is compromised due to such reasons. Significant discrepancies are particularly evident for 1s.

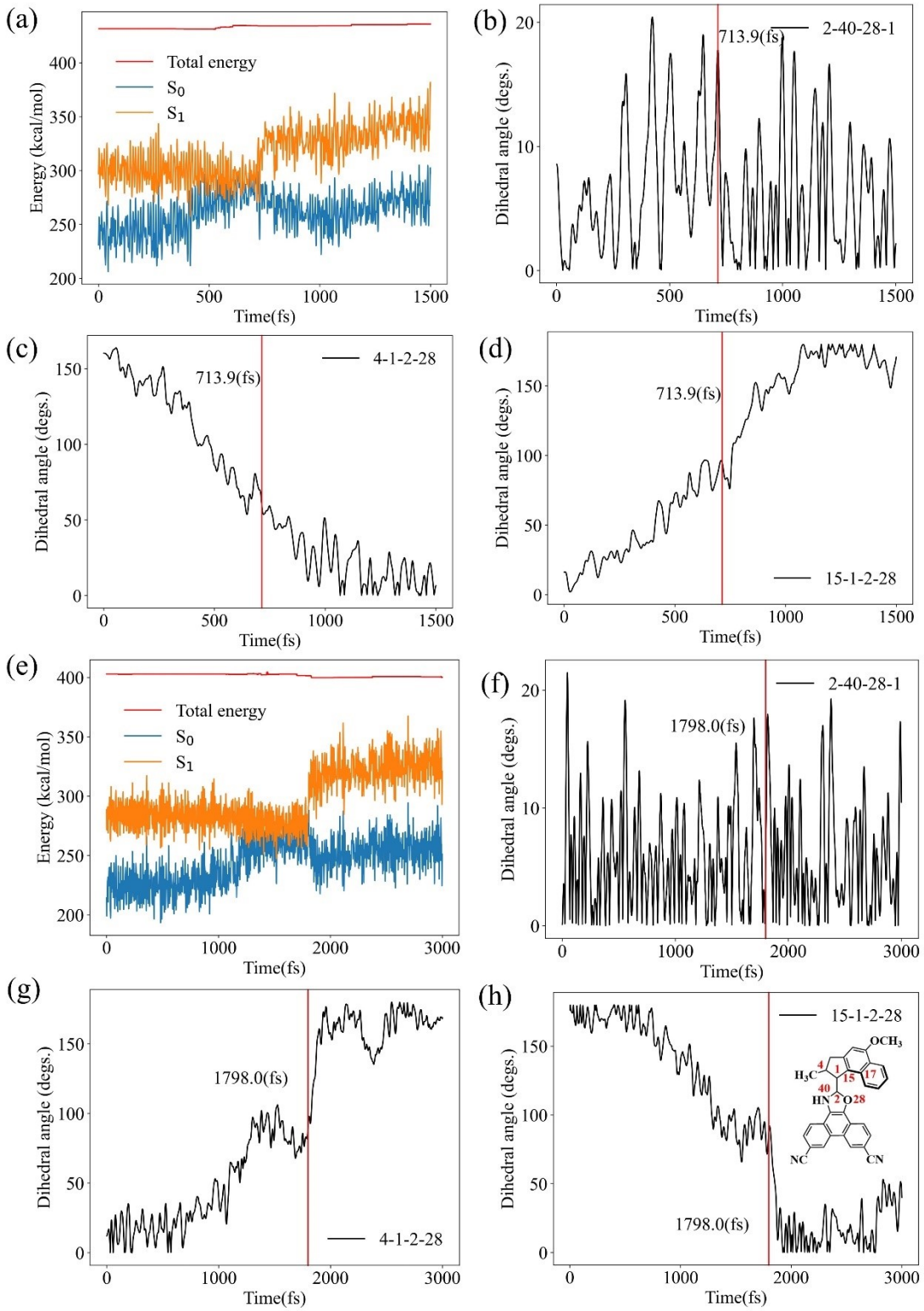

Figure S11. (a) Variation of S_0 and S_1 energies and (b-d) variations of the dihedral angles $\theta_{2\text{-}40\text{-}28\text{-}1}$, $\theta_{4\text{-}1\text{-}2\text{-}28}$, and $\theta_{15\text{-}1\text{-}2\text{-}28}$, along a typical trajectory for Xs-EP; (e) Variation of S_0 and S_1 energies and (f-h) variations of the dihedral angles $\theta_{2\text{-}40\text{-}28\text{-}1}$, $\theta_{4\text{-}1\text{-}2\text{-}28}$, and $\theta_{15\text{-}1\text{-}2\text{-}28}$, along a typical trajectory for Xs-ZP.

To gain a thorough insight into the isomerization mechanism, we explore two representative trajectories, namely EP → ZM and ZP → EM, which represent pivotal transitions within the molecular motor's isomerization processes. Starting with EP → ZM, the journey begins as the EP isomer is energetically uplifted to the S_1 state, setting the molecular motor on a path across the excited-state potential energy landscape until it descends back to the ground state at 713.9 fs. Illustrated in Figure S11(b-d), this path witnesses the dihedral angle $\theta_{4\text{-}1\text{-}2\text{-}28}$, a critical link between the rotor and stator, ascend from its optimized EP form, experiencing fluctuations to stabilize at a 20° inclination by 713.9 fs. Concurrently, the dihedral angle $\theta_{15\text{-}1\text{-}2\text{-}28}$ exhibits a gradual decrement. Notably, the dihedral angle $\theta_{2\text{-}40\text{-}28\text{-}1}$ sees a swift increase, heralding the trajectory's venture into the CI region, alongside a pronounced pyramidalization at the carbon atom nestled within the stator-axle. The culmination of this photoisomerization sequence is signified by the dihedral angles $\theta_{4\text{-}1\text{-}2\text{-}28}$ and $\theta_{15\text{-}1\text{-}2\text{-}28}$ achieving equilibrium.

Turning our focus to the ZP → EM transition depicted in Figure S11(f-h), the narrative unfolds with the dihedral angle $\theta_{4\text{-}1\text{-}2\text{-}28}$ embarking from its initial stance, navigating through CI geometries at 1798.0 fs, before gracefully transitioning to the ground state. This relaxation phase sees the dihedral angle $\theta_{15\text{-}1\text{-}2\text{-}28}$ diminish from the ZP isomer's 170°, alongside a significant swell in the dihedral angle $\theta_{2\text{-}40\text{-}28\text{-}1}$, a movement that underscores the carbon atom's pyramidalization at the stator-axle. Impressively, the dihedral angle $\theta_{4\text{-}1\text{-}2\text{-}28}$ escalates from a modest 20° in ZP to a striking 170° throughout the ZP → EM isomerization, leading to a successful conclusion as the dihedral angles $\theta_{4\text{-}1\text{-}2\text{-}28}$ and $\theta_{15\text{-}1\text{-}2\text{-}28}$ stabilize at predetermined coordinates, effectively charting the isomerization's course.

9. Simulated time-dependent fluorescence and dark state

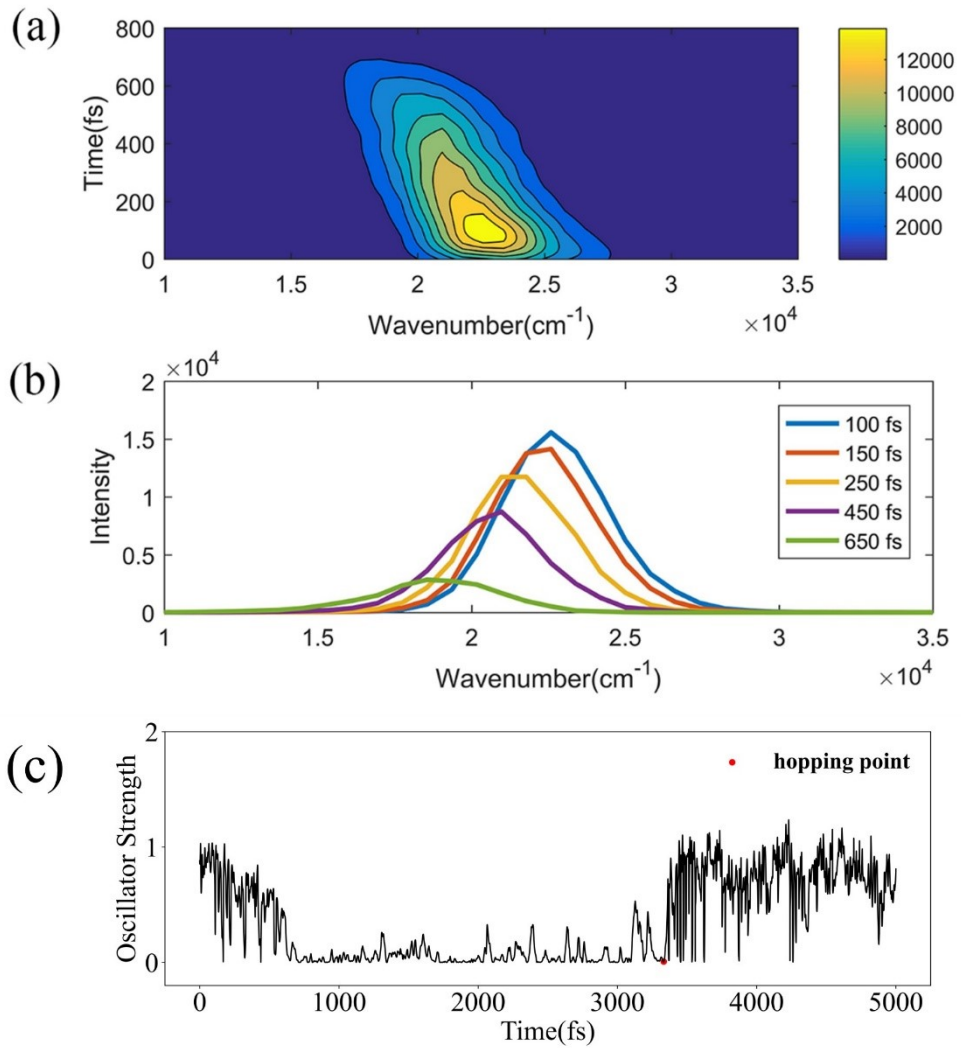

Figure S12. The simulated time-dependent fluorescence emission spectrum of 1s: (a) a two-dimensional contour plot that illustrates the emission intensity in relation to both the simulation time and the wavenumber of photons; (b) fluorescence emission spectrum at various times; (c) The oscillator strength between the ground state (S_0) and the first excited state (S_1). The hopping time is displayed by a red point.

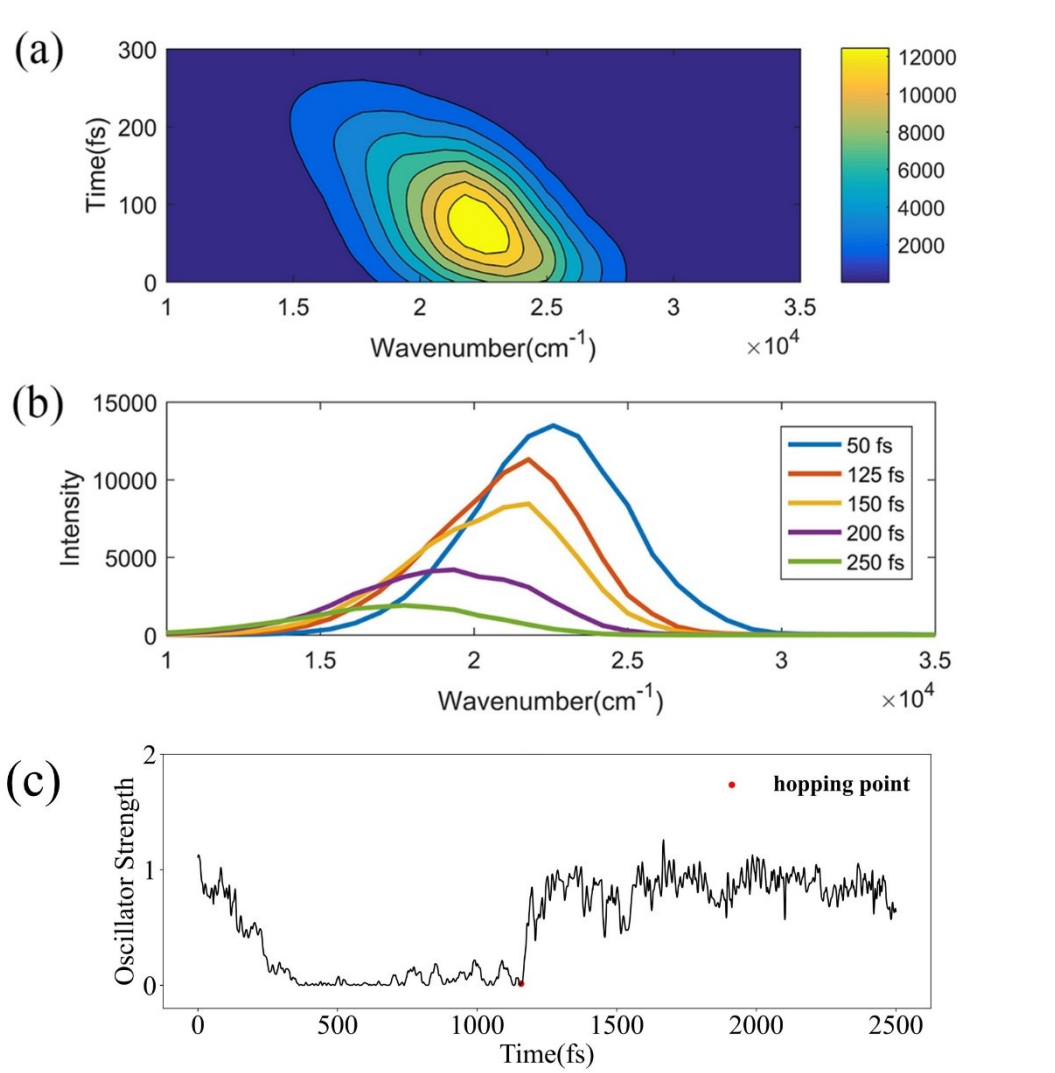

Figure S13. The simulated time-dependent fluorescence emission spectrum of 2s: (a) a two-dimensional contour plot that illustrates the emission intensity in relation to both the simulation time and the wavenumber of photons; (b) fluorescence emission spectrum at various times; (c) The oscillator strength between the ground state (S_0) and the first excited state (S_1). The hopping time is displayed by a red point.

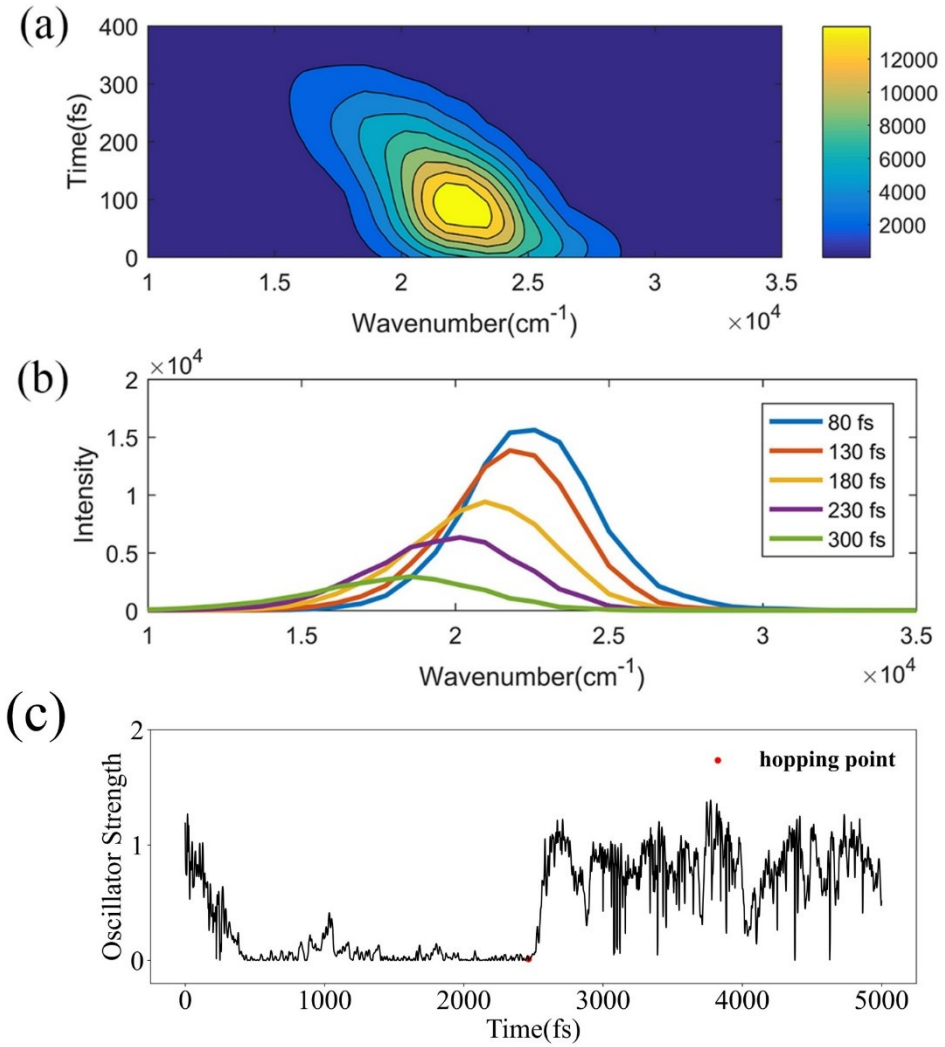

Figure S14. The simulated time-dependent fluorescence emission spectrum of 6s: (a) a two-dimensional contour plot that illustrates the emission intensity in relation to both the simulation time and the wavenumber of photons; (b) fluorescence emission spectrum at various times; (c) The oscillator strength between the ground state (S_0) and the first excited state (S_1). The hopping time is displayed by a red point.

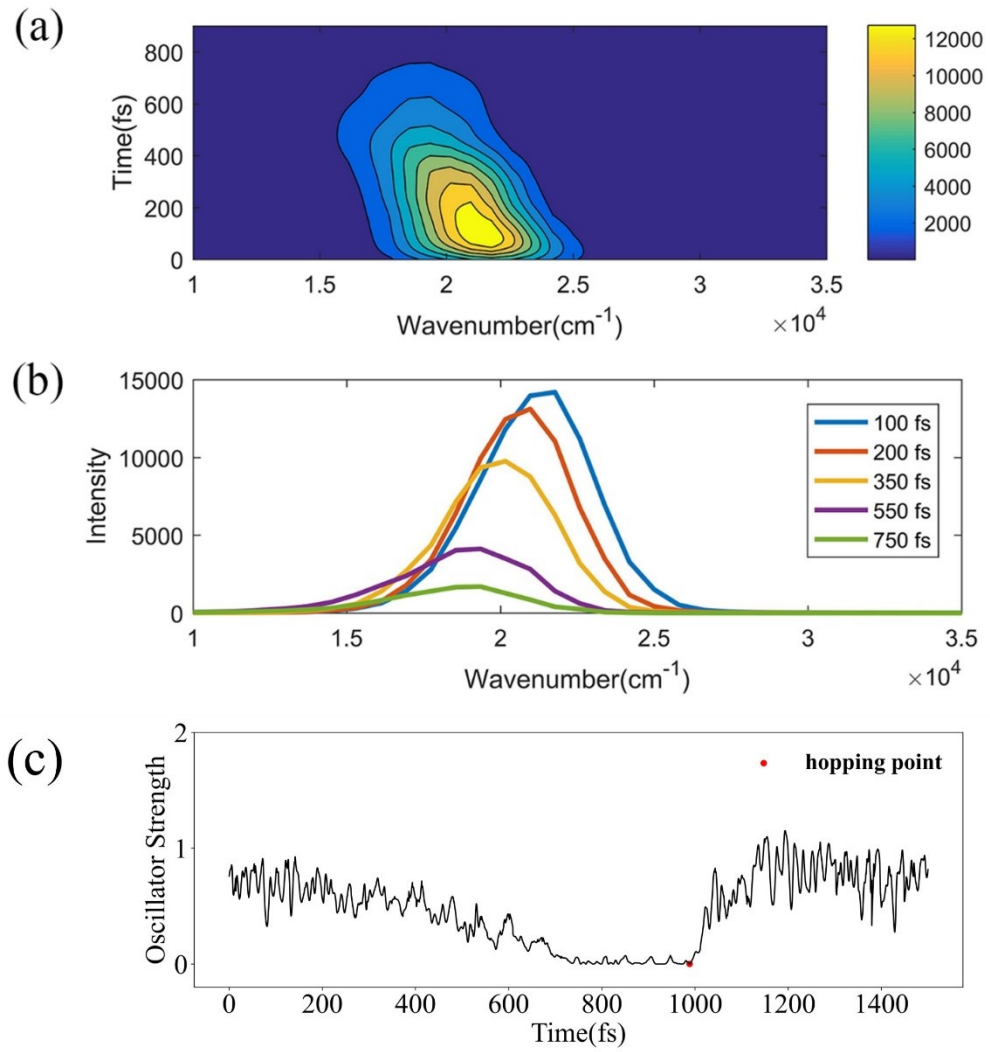

Figure S15. The simulated time-dependent fluorescence emission spectrum of Xs-EP: (a) a two-dimensional contour plot that illustrates the emission intensity in relation to both the simulation time and the wavenumber of photons; (b) fluorescence emission spectrum at various times; (c) The oscillator strength between the ground state (S_0) and the first excited state (S_1). The hopping time is displayed by a red point.

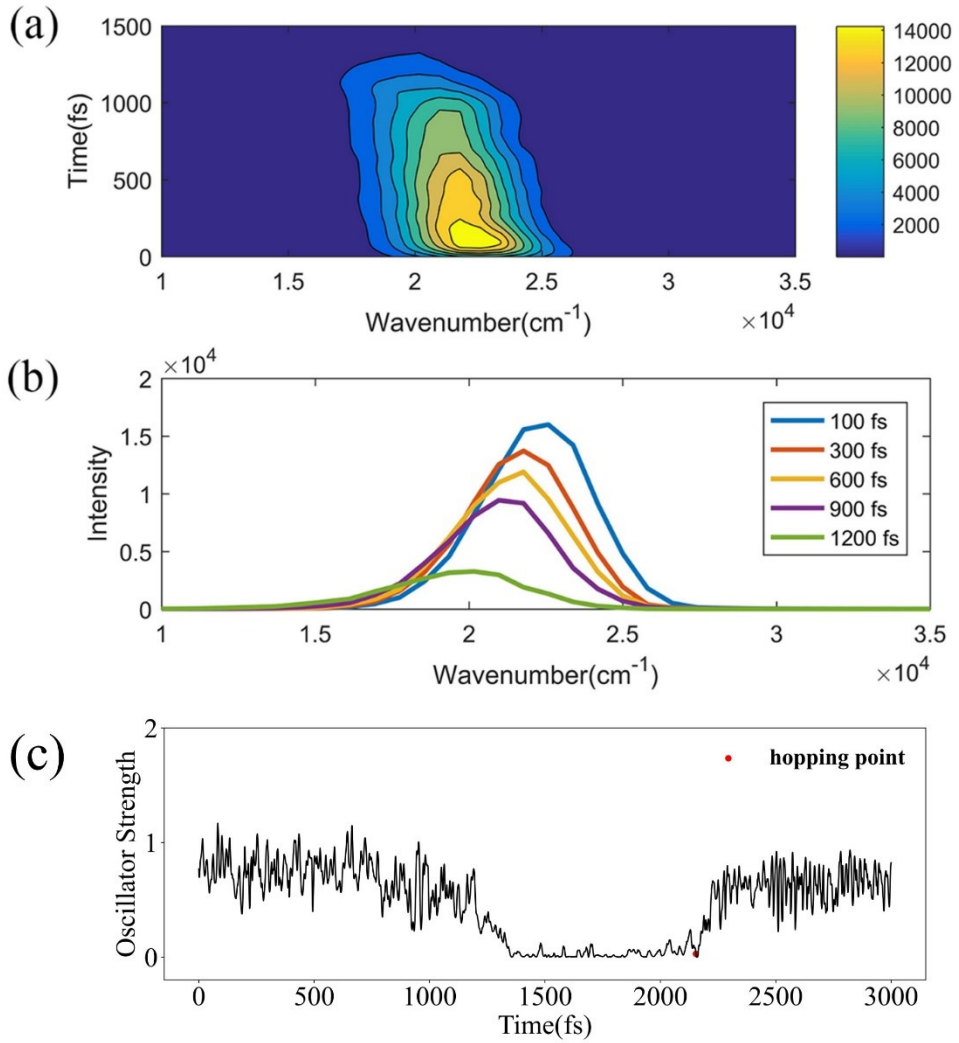

Figure S16. The simulated time-dependent fluorescence emission spectrum of Xs-ZP: (a) a two-dimensional contour plot that illustrates the emission intensity in relation to both the simulation time and the wavenumber of photons; (b) fluorescence emission spectrum at various times; (c) The oscillator strength between the ground state (S_0) and the first excited state (S_1). The hopping time is displayed by a red point.

Table S15. The average lifetime, the time of fluorescence emission quenching, and dark state duration for four motors.

		Average lifetime (ps)	Time of fluorescence emission quenching (ps)	Dark state duration (ps)
1s	P	2.56	0.70	1.86
2s	P	1.16	0.26	0.90
6s	P	2.40	0.34	2.06
Xs	EP	0.85	0.76	0.09
	ZP	1.58	1.32	0.26

The time-resolved fluorescence emission spectrum during the P → M (1s, 2s, 6s) and EP → ZM, ZP → EM (Xs) photoisomerization processes were computed using 175, 242, 233 trajectories for 1s-P, 2s-P, 6s-P, respectively, and 220 and 179 trajectories for Xs-EP and XS-ZP within our simulations. These calculations stem from nonadiabatic dynamics simulation outcomes, factoring in state energy, oscillator strengths, and the instantaneous electronic state of all trajectories throughout the simulation. To calculate the fluorescence intensity at each point in time, we employed a 10 fs time step, aggregating the oscillator strengths of all trajectories that remained in the excited state at that moment. It's worth mentioning that this calculation approach is succinctly outlined here; for a more comprehensive theoretical framework, readers are encouraged to consult the works of Lan *et al.*[5] and Jin *et al.*[6]

The emission intensity $I(\omega,t)^{\text{emission}}$ at time t is calculated as follows:

$$I(\omega,t)^{emission} \propto \omega^3 \sum_{i=1}^{N_1} f(\omega_i,t)\delta(\omega-\omega_i)$$

Here, $f(\omega_i, t)$ represents the oscillator strength of the ith trajectory at time t, and N_1 is the number of trajectories remaining in the S_1 excited state. The cumulative emissions over time and frequency domains are given by

$$I(t)^{emission} = \int I(\omega,t)^{emission} d\omega$$

and

$$I(\omega)^{emission} = \int I(\omega,t)^{emission} dt$$

The two-dimensional contour plot displaying the fluorescence emission intensity across both time and frequency domains are shown in Figures S12(a), S13(a), and S14(a) for 1s-P, 2s-P, and 6s-P, and in Figures S15(a) and S16(a) for Xs-EP and Xs-ZP. These plots reveal ultrafast quenching of fluorescence emissions before 700, 260, 340 fs for 1s-P, 2s-P, and 6s-P, and 760, 1320 fs for Xs-EP and Xs-ZP, alongside a noticeable red-shift in the emission photon's wavenumber. Additionally, the figures include wavelength-resolved fluorescence emission spectra at various times: 100-650, 50-250, 80-300 fs for 1s-P, 2s-P, and 6s-P, and 100-750, 100-1200 fs for Xs-EP and Xs-ZP. Taking Figure S12(b) as an instance, the central wavenumber of the emission spectrum shifts from about 1.50×10^4 cm^{-1} at 100 fs to roughly 0.25×10^4 cm^{-1} at 650 fs, with the intensity at the latter time point being significantly diminished (approximately one-sixth of its

initial value). This observation underscores the red-shift and quenching of the fluorescence emission spectrum. Given the fluorescence emission quenching times of around 700, 260, 340 fs for 1s-P, 2s-P, 6s-P, and 760, 1320 fs for Xs-EP and Xs-ZP, which are considerably shorter than the lifetimes of the S_1 excited state (2560, 1160, 2400 fs for 1s-P, 2s-P, 6s-P, and 850, 1580 fs for Xs-EP and Xs-ZP respectively), it is inferred that a "dark state" plays a role during the photoisomerization processes of these molecules. The durations of the "dark state" in the photoisomerization process, determined through nonadiabatic dynamics simulations for 1s-P, 2s-P, 6s-P, Xs-EP, and Xs-ZP, are detailed in Table S15. It's found that the "dark state" durations for 1s, 2s, and 6s span 1.86, 0.90, and 2.06 ps, markedly longer than the 0.09 and 0.26 ps for Xs-EP and Xs-ZP, respectively.

10. Active space orbitals for 1s, 2s, 6s, and Xs

1s (8,9)

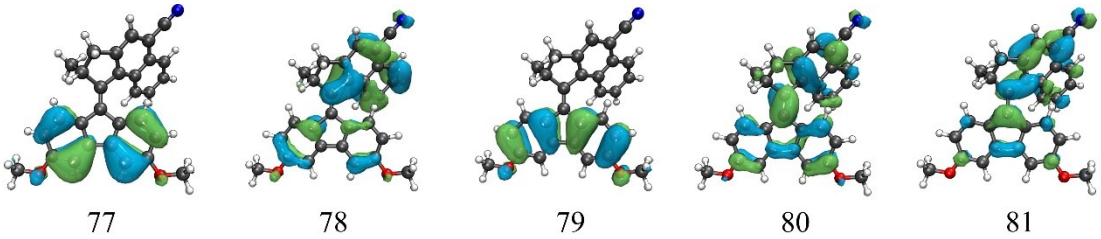

77 78 79 80 81

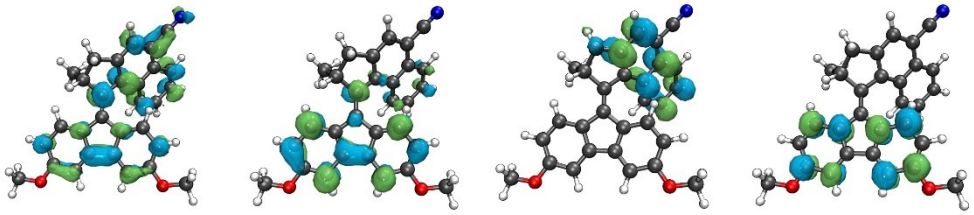

82 83 84 85

2s (10,10)

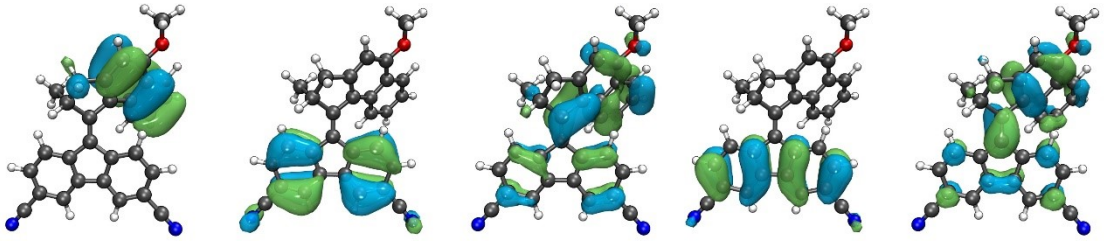

74 75 76 77 78

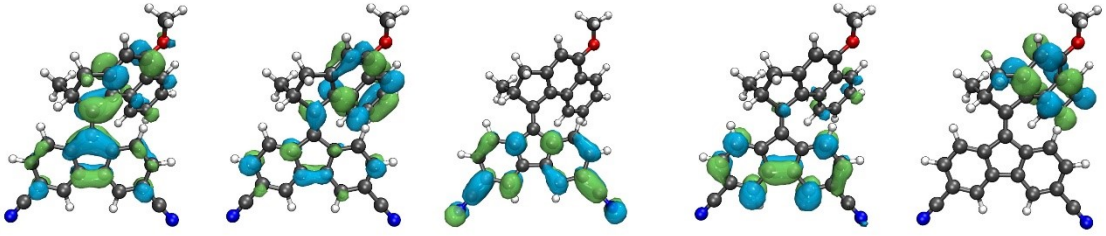

79 80 81 82 83

6s (8,8)

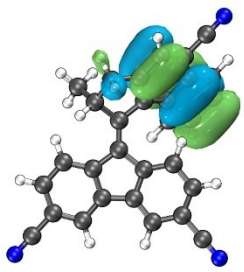

73

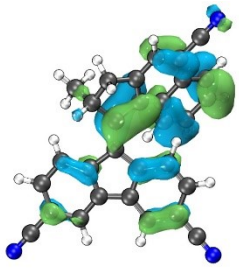

74

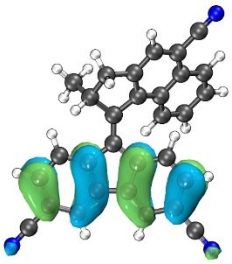

75

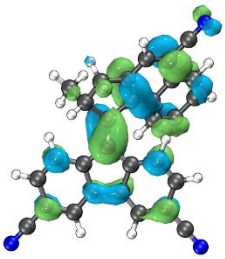

76

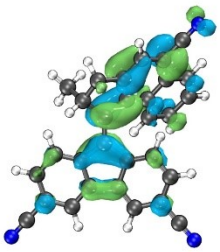

77

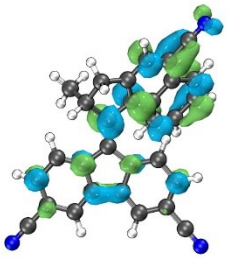

78

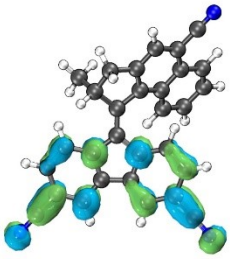

80

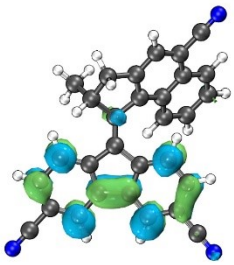

81

Xs (8,8)

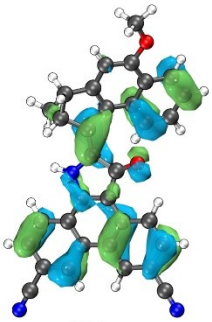

87

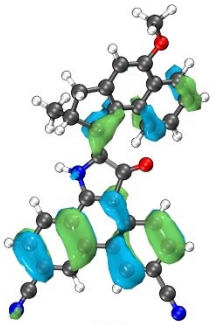

88

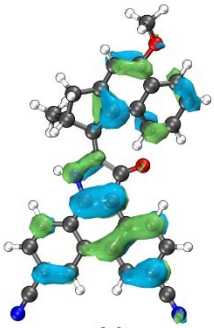

89

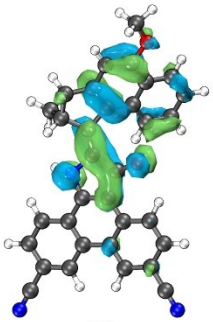

90

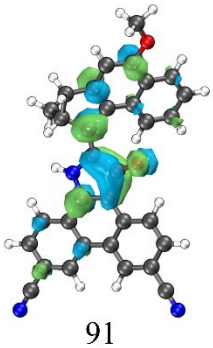

91

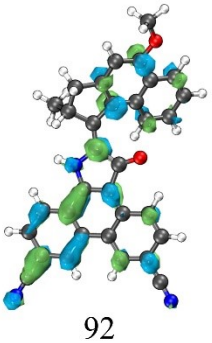

92

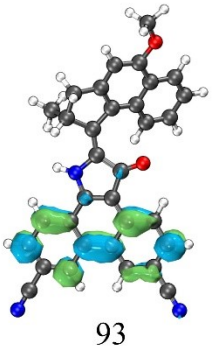

93

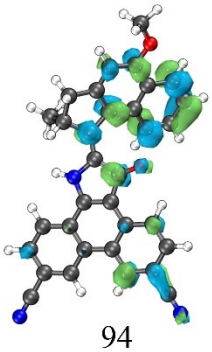

94

References

1 Thiel, W. MNDO Program, Version7.0; Max-Planck-Institut fur Kohlenforschung: Mulheim, Germany, 2007.

2 Gaussian 09, Revision D.01, M. J. Frisch, G. W. Trucks, H. B. Schlegel, G. E. Scuseria, M. A. Robb, J. R. Cheeseman, G. Scalmani, V. Barone, G. A. Petersson, H. Nakatsuji, X. Li, M. Caricato, A. V. Marenich, J. Bloino, B. G. Janesko, R. Gomperts, B. Mennucci, H. P. Hratchian, J. V. Ortiz, A. F. Izmaylov, J. L. Sonnenberg, D. Williams-Young, F. Ding, F. Lipparini, F. Egidi, J. Goings, B. Peng, A. Petrone, T. Henderson, D. Ranasinghe, V. G. Zakrzewski, J. Gao, N. Rega, G. Zheng, W. Liang, M. Hada, M. Ehara, K. Toyota, R. Fukuda, J. Hasegawa, M. Ishida, T. Nakajima, Y. Honda, O. Kitao, H. Nakai, T. Vreven, K. Throssell, J. A. Montgomery, Jr., J. E. Peralta, F. Ogliaro, M. J. Bearpark, J. J. Heyd, E. N. Brothers, K. N. Kudin, V. N. Staroverov, T. A. Keith, R. Kobayashi, J. Normand, K. Raghavachari, A. P. Rendell, J. C. Burant, S. S. Iyengar, J. Tomasi, M. Cossi, J. M. Millam, M. Klene, C. Adamo, R. Cammi, J. W. Ochterski, R. L. Martin, K. Morokuma, O. Farkas, J. B. Foresman, and D. J. Fox, Gaussian, Inc., Wallingford CT, 2013.

3 L. Pfeifer, M. Scherübl, M. Fellert, W. Danowski, J. Cheng, J. Pol and B. L. Feringa, Photoefficient 2nd generation molecular motors responsive to visible light, *Chem Sci*, 2019, **10**, 8768–8773.

4 M. Barbatti, M. Bondanza, R. Crespo-Otero, B. Demoulin, P. O. Dral, G. Granucci, F. Kossoski, H. Lischka, B. Mennucci, S. Mukherjee, M. Pederzoli, M. Persico, M. Pinheiro Jr, J. Pittner, F. Plasser, E. Sangiogo Gil and L. Stojanovic, Newton-X Platform: New Software Developments for Surface Hopping and Nuclear Ensembles, *J Chem Theory Comput*, 2022, **18**, 6851–6865.

5 Z. Lan, Y. Lu, O. Weingart and W. Thiel, Nonadiabatic Decay Dynamics of a Benzylidene Malononitrile, *J Phys Chem A*, 2012, **116**, 1510–1518.

6 H. Jin, M. Liang, S. Arzhantsev, X. Li and M. Maroncelli, Photophysical Characterization of Benzylidene Malononitriles as Probes of Solvent Friction, *J Phys Chem B*, 2010, **114**, 7565–7578.